Catalysis Science & Technology

PAPER

Cite this: *Catal. Sci. Technol.*, 2016, **6**, 6879

A combined theoretical and experimental EXAFS study of the structure and dynamics of Au_{147} nanoparticles

Zhiyao Duan,†[a] Yuanyuan Li,†[b] Janis Timoshenko,[b] Samuel T. Chill,[a] Rachel M. Anderson,[c] David F. Yancey,[c] Anatoly I. Frenkel,*[b] Richard M. Crooks*[c] and Graeme Henkelman*[a]

Received 13th March 2016,
Accepted 25th May 2016

DOI: 10.1039/c6cy00559d

www.rsc.org/catalysis

In this study, we present a framework for characterizing the structural and thermal properties of small nanoparticle catalysts by combining precise synthesis, extended X-ray absorption fine structure (EXAFS) spectroscopy, and density functional theory (DFT) calculations. We demonstrate the capability of this approach by characterizing the atomic structure and vibrational dynamics of Au_{147}. With the combination of EXAFS spectroscopy and DFT, the synthesized Au_{147} nanoparticles are determined to have an icosahedral structure. A decrease in the Einstein temperature of the Au_{147} particles compared to their bulk value was observed and interpreted in terms of softer vibration modes of surface bonds.

1 Introduction

While bulk Au is considered inert, small Au nanoparticles with diameters less than 5 nm are surprisingly active for specific chemical reactions.[1–3] There is evidence showing that the number of low-coordinated Au atoms scales approximately with the catalytic activity for CO oxidation, suggesting that atoms on the corners and edges of Au nanoparticles are the active sites.[3,4] Accordingly, we can expect that the catalytic activity of Au nanoparticles would be strongly dependent on morphology, and both the number and the coordination number of those undercoordinated Au atoms. The vibrational dynamics of surface atoms was also shown to have a strong effect on their catalytic activity.[5–7] Additional interest in dynamics stems from the theoretical and experimental reports[8–10] that small clusters have a lower melting temperature than the bulk and thus, according to the Lindemann criterion,[11] lower Debye and Einstein temperatures as well. These facts put a strong demand on the accurate characterization of Au nanoparticle structures and dynamics in order to establish structure–function relationships. However, the inherently small length scale and enhanced structural disorder of small nanoparticles limit the application of traditional diffraction methods and electron microscopy.

Extended X-ray absorption fine structure (EXAFS) spectroscopy stands out in characterizing small metal nanoparticles due to its local nature; only distances within 6–8 Å of the photo-absorbing atoms are probed. The structural information on the measured metal nanoparticles, such as coordination numbers, interatomic distances, and bond length disorder, can be obtained by fitting the structural parameters of the simulated system to match the EXAFS spectrum. However, we have previously demonstrated that this fitting approach can lead to problems in the interpretation of the structural information from the spectrum especially when significant asymmetric structural disorder is caused by surface tension and other effects such as interactions with ligands and supports.[12,13]

An approach to avoid the above-mentioned drawback of the conventional EXAFS analysis uses first-principles methods to directly simulate the EXAFS spectrum without any parameterizations. By comparing the simulated EXAFS spectra of different candidate structures with the experimental data, structures that are consistent with the synthesized sample can be determined. Additionally, the total energies of candidate structures can be readily calculated with the first-principles methods, providing an additional metric for selection in the structure determination process. Once the structure of the system under measurement is determined, its structural and vibrational properties can be determined with full atomic resolution from the theoretical model.

Direct experimental characterization of the structure and dynamics of small nanoparticles requires measurements *in situ* of well-defined atomic clusters that are free from competing effects of supports and adsorbates and thus exceedingly

[a] *Department of Chemistry and the Institute for Computational Engineering and Sciences, The University of Texas at Austin, Austin, TX 78712-0165, USA. E-mail: henkelman@utexas.edu; Fax: 512 471 8696; Tel: 512 471 4179*
[b] *Physics Department, Yeshiva University, 245 Lexington Avenue, New York, NY 10016, USA. E-mail: anatoly.frenkel@yu.edu*
[c] *Department of Chemistry, The University of Texas at Austin, Austin, TX 78712-0165, USA. E-mail: crooks@cm.utexas.edu*
† These authors contributed equally to this work.

difficult to synthesize. Dendrimer encapsulated nanoparticles (DENs) are attractive because they are not immobilized on supports and because metal clusters are only weakly interacting with the dendrimers,[14] hence the metal bonding structure and intrinsic cluster size effects on bond dynamics can be investigated in greater detail. DENs also represent an ideal system for the purpose of computational modeling for they have been demonstrated to exhibit remarkable size and structural monodispersity,[15] allowing them to be analyzed with a single atomistic model.

In this study, we applied the combined EXAFS and first-principles framework to explore the structural and vibrational properties of Au_{147} DENs. Although the study on the effects of structural disorder on EXAFS spectra by comparing first-principles calculations and experimental data has been done by us and others before,[12,13,16,17] here we are focusing on the bond length disorder caused by dynamic effects.

2 Methods

2.1 Experimental details

Solutions of 50 mL of 2 μM Au_{147} DENs were synthesized as previously reported.[18] Sixth-generation amine-terminated (G6-NH2) poly(amidoamine) dendrimers (Dendritech) were used at a concentration of 2 μM, and 147 equiv. of $HAuCl_4$ salt was added. This solution was stirred for 10 minutes, after which a 10-fold excess of $NaBH_4$ was added in 3.0 mL of a 0.30 M NaOH solution. The resulting DEN solution was stirred in air for at least 12 hours to allow excess $NaBH_4$ to react. TEM images of Au_{147} DENs were obtained using a JEOL 2010F TEM. Carbon-coated copper TEM grids (400 mesh) were purchased from Electron Microscopy Sciences. TEM grids were prepared by dropping 3.0 μL of the 2.0 μM DEN solution onto the grid and allowing it to dry in air.

For EXAFS measurements, the solutions were frozen in liquid N_2 and freeze-dried in a Labconco FreeZone 12 lyophilizer. The dried DEN powder was pressed into a pellet and used for the temperature studies. EXAFS experiments were carried out at the National Synchrotron Light Source (Brookhaven National Laboratory) at beamline X18B. Au L3-edge data were collected in transmission mode using gas ionization detector chambers. The temperature was controlled by a closed cycle Displex cryostat. Due to the temperature gradients observed during the measurements, the nanoparticle sample and the foil were placed on the same sample holder and measured under the same conditions.

2.2 EXAFS fitting details

EXAFS data modeling and analysis were done using established procedures. Briefly, the Au foil EXAFS was analyzed first, using a multiple data set scheme where all the data collected at multiple temperatures were fit to FEFF6 theory simultaneously and several constraints were applied to minimize the number of variables in the fit and reduce the correlation of fitting parameters. The passive electron reduction factor was obtained as 0.879 and fixed in the fits of nanoparticle data. Those temperature values were subsequently fixed for the analysis of the nanoparticle data. Then, we performed analysis in two different ways. First, we treated all Debye–Waller factors independently in the fit. Next, we constrained them in the fitting process to follow the Einstein model. In both cases the coordination number and ΔE were constrained to be the same at all temperatures. As a result, the measurements of Einstein temperatures, static disorder values and Au–Au bond distances were obtained in both the bulk Au and the nanoparticle sample. The third cumulant was found not to affect the fit results, within the error bars, and was then constrained to be zero at all temperatures to improve the uncertainty of the fit.

2.3 Computational details

The theoretical calculations were done using density functional theory (DFT) implemented in the Vienna *ab initio* simulation package (VASP).[19,20] All calculations were spin-polarized. Core electrons were described with the projector augmented-wave (PAW) method.[21,22] The Kohn–Sham wave functions for the valence electrons were expanded in a plane-wave basis set with an energy cutoff of 300 eV. The exchange–correlation energy was treated within the framework of the generalized gradient approximation. Specifically, PBEsol[23] was used, which is a modified form of the Perdew–Burke–Ernzerhof (PBE) functional designed to improve lattice parameters and surface energies in solids. A single Γ-point was sufficient for integration of the reciprocal space due to the finite nature of the nanoparticles. A unit cell of 5 × 5 × 5 was used to model the Au bulk and simulate the EXAFS spectrum for the Au foil. A *k*-point mesh of 2 × 2 × 2 was used for this periodic model.

To simulate the EXAFS spectrum, an ensemble of equilibrium structures at finite temperatures is required. To avoid direct sampling of equilibrium structures based upon our DFT calculations, we constructed and sampled a DFT-derived harmonic potential. Employing a harmonic potential improves the efficiency of our temperature-dependent study because once the potential is derived it can be used to sample structures at different temperatures without additional DFT calculations. In addition, the harmonic potential approach is suitable for studying metastable structures, which could transform to more stable structures during a molecular dynamics or Monte Carlo sampling simulation, and low temperatures where the use of the quantum partition function is more accurate than the classical one. This harmonic approximation of the potential energy surface was found to be appropriate for the temperatures of interest below 300 K, and not affect our results. Dynamical matrices for the Au nanoparticles were obtained using a finite difference method in which a small displacement of 0.01 Å was applied to every degree of freedom of the equilibrium structure. A set of $3N - 6$ harmonic oscillators with their force constant and vibrational normal modes were obtained by diagonalizing

the dynamical matrix. Statistically independent structures at finite temperature were then sampled by displacing the atoms in the nanoparticle along each normal mode with a magnitude following a Gaussian distribution. The standard deviation of the Gaussian distribution was taken to be $\sqrt{(\hbar/2M_{Au}\omega)\coth(\hbar\omega/2k_BT)}$, which is the variance of the position of a quantum harmonic oscillator. In the equation, M_{Au} is the mass of an Au atom, ω is the vibrational frequency, $\hbar$ is Planck's constant, k_B is Boltzmann's constant, and T is the temperature.

Based on the set of structures at finite temperatures, theoretical EXAFS signals were simulated using an approach similar to that reported previously.[18] The Au L3-edge EXAFS spectra were calculated from 800 structures by averaging the signal arising from each Au atom in the NP. The multiple-scattering calculations were performed using FEFF6-lite.[24] All atoms up to 6.0 Å away from each photo-absorbing atom were included in the scattering calculations. The experimental correction to the photoelectron energy origin and the passive electron reduction factor was applied to the simulated EXAFS spectra to align experimental and theoretical data in k-space.

To analyze the vibrational properties of Au_{147}, we employed the equation of motion (EM) method to calculate the bond-projected vibrational density of states (VDOS).[25,26] In this method, the projected VDOS is calculated as a cosine transform of the displacement–displacement time-correlation function $\langle Q_R(t)|\ Q_R(0)\rangle$ with an exponential damping factor,

$$\rho_R(\omega) = \frac{2}{\pi}\int_0^{t_{max}} \langle Q_R(t)\,|\,Q_R(0)\rangle \cos\omega t e^{-\varepsilon t^2}\,dt. \quad (1)$$

Here, $|Q_R(0)\rangle$ is the initial displacement state vector, in which a selected nearest-neighbor bond (first-shell scattering path) is perturbed. The displacement state $\langle Q_R(t)|$ is determined by running micro-canonical molecular dynamics using the DFT-derived harmonic potential. Newton's equations of motion are integrated using the Verlet velocity algorithm with a time step of 1 fs and a total simulation time of 10 ps. The spectral width is determined by the cutoff parameter $\varepsilon = 3/t_{max}^2$. In this work t_{max} is chosen to be 10 ps. Once the projected VDOS $\rho_R(\omega)$ is obtained, the mean-square relative displacement, which is described as the Debye–Waller factor σ^2, for a given scattering path R is given by the Debye integral

$$\sigma_R^2 = \frac{\hbar}{2\mu_R}\int_0^{\omega_{max}} \frac{d\omega}{\omega}\rho_R(\omega)\coth\frac{\beta\hbar\omega}{2} \quad (2)$$

where μ_R is the reduced mass associated with the path. For the nearest-neighbor bonds considered in this work, $\mu_R = M_{Au}/2$. The total projected VDOS is obtained by iterating over all pairs of bonds in the system.

3 Results and discussion

3.1 Morphological characterization

The size distribution and morphology of the synthesized Au_{147} DENs were obtained from TEM images. Fig. 1 shows a representative TEM image for the Au_{147} DENs as well as a histogram showing that the average diameter of the nanoparticles is 1.6 ± 0.2 nm. The Au_{147} DENs are highly monodispersed so they could be represented by the single atomic model used in our DFT calculations.

3.2 EXAFS first-shell fitting

Structural information on the Au foil and Au_{147} at temperatures between 0 and 300 K was extracted by fitting the experimental EXAFS spectra. The fitted structural parameters including the coordination number (N), the average Au–Au bond length (R), and the EXAFS Debye–Waller factor (σ^2) are reported in Table 1. The temperature-dependent σ values are constrained to follow the correlated Einstein model,[27,28]

$$\sigma^2(T) = \sigma_s^2 + \frac{\hbar^2}{2k_B\mu}\frac{1}{\Theta_E}\coth\frac{\Theta_E}{2T}, \quad (3)$$

where μ is the reduced mass of the Au–Au bond. In this way, we can obtain the static Debye–Waller factor (σ_s^2) and the Einstein temperature $\left(\Theta_E \equiv \frac{\hbar\omega}{k_B}\right)$. Note that the validity of using the Einstein model approximation is validated later both by fitting the experimental EXAFS spectra without the constraint of eqn (3) and by comparison to theory, which also does not assume the Einstein model.

It is evident that the decrease in size from the Au foil to Au_{147} leads to the reduction in the coordination number, the average bond length, and increase in the bond length disorder. The increased Debye–Waller factor comes both from static and vibrational contributions. Au_{147} DENs possess sizable σ_s^2, which is a manifestation of the deviations of the average atomic positions in the nanoparticles from the perfect FCC structure. The Einstein temperature is lower for Au_{147} DENs compared to that of the Au foil which corresponds to enhanced vibrational disorder in the nanoparticle.

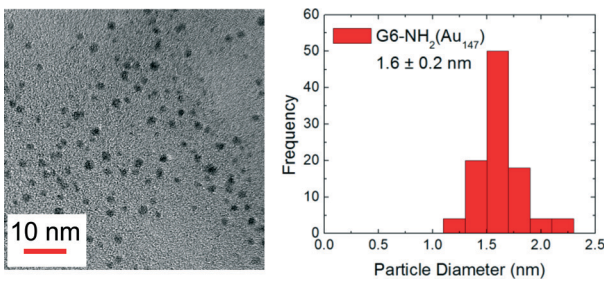

Fig. 1 TEM image and size-distribution histogram of Au_{147} DENs.

Table 1 Structural parameters obtained by fitting of the experimental EXAFS data

	T (K)	N	R (Å)	σ^2 (10^{-3} Å^2)
Au foil	52	12	2.870(2)	2.2
	84	12	2.870(2)	2.9
	98	12	2.869(2)	3.2
	146	12	2.868(2)	4.3
	202	12	2.871(2)	5.8
	250	12	2.872(3)	7.1
	295	12	2.875(3)	8.3
	σ_s^2 = 0.10 ± 0.04 (10^{-3} Å^2)		Θ_E = 134.5 ± 0.8 (K)	
Au_{147}	149	8.8	2.824(4)	9.9
	157	8.8	2.821(6)	10.1
	167	8.8	2.826(5)	10.4
	175	8.8	2.820(4)	10.6
	215	8.8	2.817(5)	11.9
	242	8.8	2.811(4)	12.7
	298	8.8	2.818(5)	14.4
	σ_s^2 = 4.9 ± 0.9 (10^{-3} Å^2)		Θ_E = 124.9 ± 9.4 (K)	

3.3 Structure determination for Au_{147} DENs

The above analysis through model fitting provides insights into the nanoparticle structure and vibrational properties. However, no direct knowledge about the atomic structure of the Au_{147} DENs could be obtained. In this section, the atomic structure of Au_{147} DENs is probed by comparing the simulated and experimental EXAFS spectra.

We first benchmark our simulation method by reproducing the EXAFS spectrum for the Au foil where the atomic structure is known exactly. The simulated and measured EXAFS spectra for the Au foil at two temperatures are compared in Fig. 2. The agreement with experiments is satisfactory. Based on this foundation, the simulation method was used for the structural determination of the Au_{147} DENs. However, before moving to the analysis of the nanoparticle structures, we further evaluated quantitatively the systematic error of our DFT-based simulation in reproducing the experimental EXAFS spectrum of the Au foil. To estimate the systematic error, we compared the structural parameters of the Au foil obtained from fitting both the experimental and simulated EXAFS spectra using the same fitting ranges and parameters. Although the theoretical structural parameters can also be obtained directly from the atomic models, we chose the fitting analysis to avoid ambiguity when comparing the data from different methods. In the analysis, we constrained the amplitude reduction factor to 0.879 to reduce the uncertainty of the fit and released the constraints on the Debye–Waller factors to follow the Einstein model. Due to the different fitting constraints, the fitted structural parameters are expected to be slightly different from those reported in Table 1. At 146 K, the theoretical σ^2 is fitted to be 4.75 ± 0.03 × 10^{-3} Å^2; the value is larger than the fitted experimental value (4.45 ± 0.04 × 10^{-3} Å^2) by 0.3 × 10^{-3} Å^2. At 295 K, the theoretical value of σ^2 (8.90 ± 0.08 × 10^{-3}Å^2) is larger than the experimental value (8.25 ± 0.10 × 10^{-3}Å^2) by about 0.6 × 10^{-3}Å^2. These results show that the Debye–Waller factors are consistently overestimated by about 7% in our DFT-based simulation. The systematic errors are also present in the fitted interatomic distances. In the simulation, the Au–Au bond lengths in the first coordination shell are overestimated by about 0.022 Å. Bearing these systematic errors of our simulation method in mind, we compare the simulated and experimental EXAFS spectra to analyze the nanoparticle structures.

Two structures were considered for the Au_{147} nanoparticles: icosahedral and cubo-octahedral. These structures were chosen because they are the two highly-symmetric structures with the magic number of 147 atoms. The atomic models of these two structures are shown in Fig. 3. The simulated and experimental EXAFS spectra for Au_{147} are shown in Fig. 4. From the data in R-space, it can be seen that the cubo-octahedral structure is more ordered (corresponding peaks in R-space are narrower) than the icosahedral structure. Fig. 5(a) shows that the pair distribution function (PDF) of the cubo-octahedral structure has a narrower distribution of the first-neighbor bond lengths compared to the icosahedral structure. The disorder in the icosahedral structure is a consequence of the twinning defects while the cubo-octahedral structure has regular FCC packing. In addition, the less distorted nature of the cubo-octahedral structure is not a result of the systematic error of our simulation method since

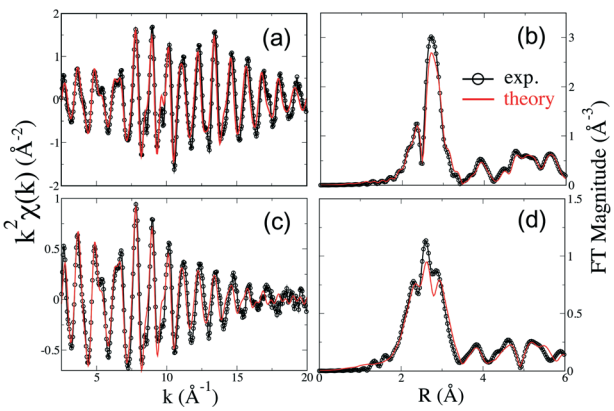

Fig. 2 Comparison between the simulated (red line) and experimental (black line) EXAFS spectra and the corresponding Fourier transforms of Au foil at two representative temperatures 146 K ((a) and (b)) and 295 K ((c) and (d)). The k-ranges used in the Fourier transformations are 2.5–19 Å^{-1} and 2.5–18 Å^{-1}, respectively, for 146 K and 295 K.

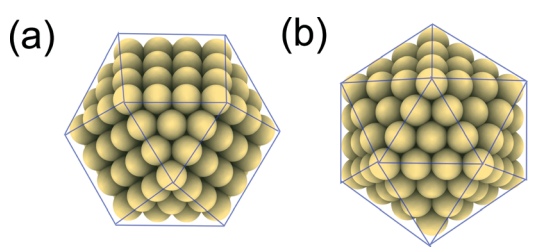

Fig. 3 Atomic structures of Au_{147} nanoparticles: (a) cubo-octahedral and (b) icosahedral.

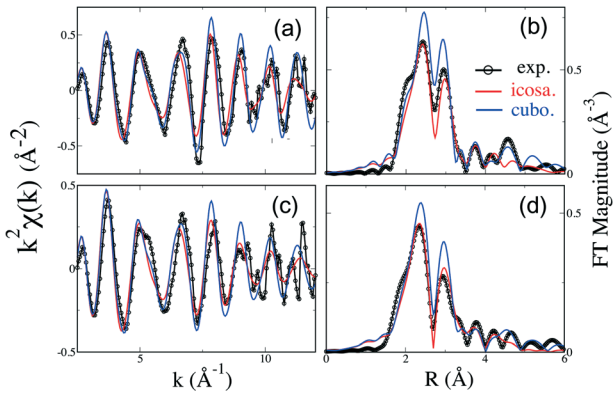

Fig. 4 Comparison between the simulated (red line for the icosahedral structure and blue line for the cubo-octahedral structure) and experimental (black line) EXAFS spectra and the corresponding Fourier transforms of the Au_{147} nanoparticles at two representative temperatures 166.6 K ((a) and (b)) and 298 K ((c) and (d)). The *k*-ranges used in the Fourier transformations are 2.5–11.6 $Å^{-1}$ and 2.5–11 $Å^{-1}$, respectively, for 166.6 K and 298 K.

the method tends to overestimate the disorder. The calculated EXAFS spectrum is closer to the experimental spectrum for the icosahedral structure in the first-neighbor region as shown in Fig. 5(b) and (c). We also noticed that the cubo-octahedral model is in better agreement for *R* between 4 Å and 5 Å, especially at lower temperatures. We tentatively attribute this to the existence of some larger nanoparticles in the sample with FCC packing. Overall, however, our comparison between the experimental and theoretical EXAFS spectra indicates that the synthesized Au_{147} DENs are more likely to be icosahedral. In addition, our DFT calculations indicate that icosahedral Au_{147} is more stable than the cubo-octahedral by 3.98 eV. In fact, a DFT-based molecular dynamics simulation of cubo-octahedral Au_{147} shows a spontaneous structural rearrangement from the cubo-octahedral to the icosahedral structure at a temperature as low as 215 K in the simulated 20 ps (using a time step of 2 fs and a Langevin thermostat), which indicates that the Au_{147} structure is not kinetically trapped as cubo-octahedral at room temperature.

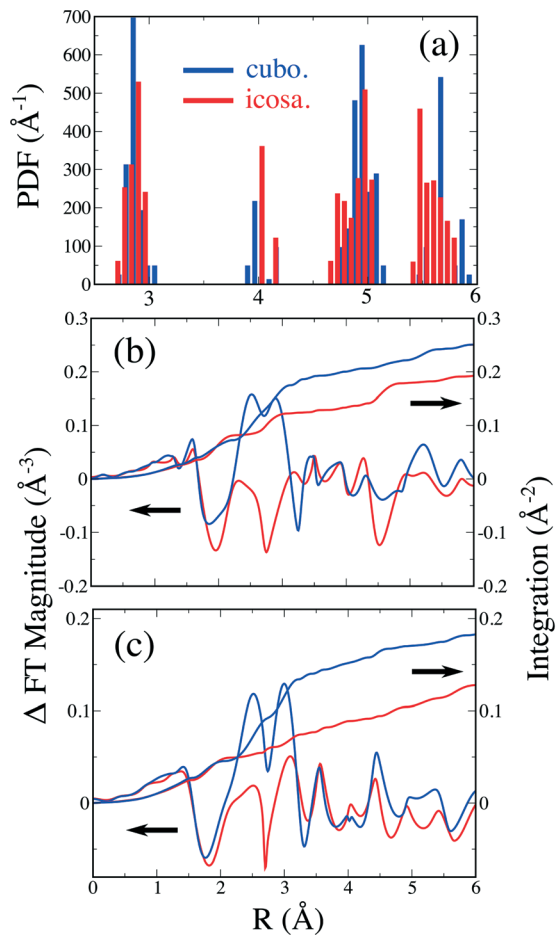

Fig. 5 (a) Pair distribution function (PDF) of cubo-octahedral and icosahedral Au_{147} nanoparticles. Differences between the real-space theoretical and experimental EXAFS spectra at 167 and 298 K are shown in (b) and (c), respectively, along with the integrated absolute difference between them.

3.4 Structural properties

Pair distribution functions (PDFs) of Au bulk and icosahedral Au_{147} obtained from DFT-sampled structures at 1 K are shown in Fig. 6. There is no significant difference between 0 and 1 K; we used the latter to avoid numerical problems with our sampling code. The Au–Au bonds in Au_{147} are categorized into three sub-groups, which are surface–surface, surface–core, and core–core bonds. The PDFs for these sub-group bonds are also included in Fig. 6. Compared to the PDF of Au bulk, the distribution of the first neighbor shell for Au_{147} is significantly broadened. On average, the bond length in Au_{147} is contracted to 2.868 Å from the bulk value of 2.879 Å. This bond contraction trend is in agreement with the fitting parameters determined from the experimental EXAFS spectra.

It should be noted that the experimentally fitted bond length for Au_{147} is shorter than that calculated directly by DFT. We attribute the discrepancy to several factors. First, there is a significant correlation between structural parameters in the EXAFS fitting model when applied to nanoparticles. Specifically, we have previously demonstrated that

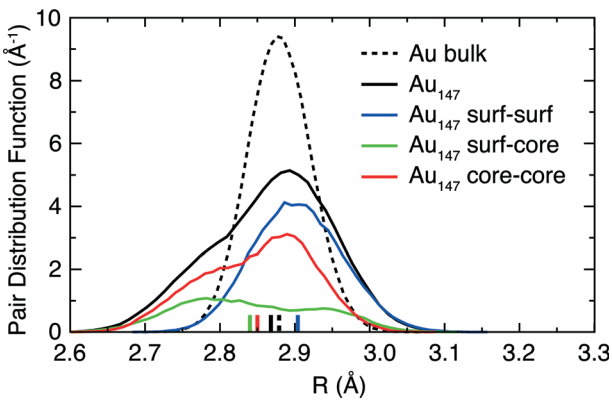

Fig. 6 Bond length distribution of Au bulk and Au_{147} extracted from the sampled structures at 1 K. The short vertical lines denote the centroids of their respective pair distribution functions.

an increase in bond length disorder (σ^2), typical for nanoparticles, can be interpreted as a decrease of *ca.* 0.04 Å in the average bond length, R.[13] A second reason for an underestimation of the experimental Au bond length is that we assumed a Gaussian distribution; including skew in the form of a third cumulant in the EXAFS fit increases the bond length by *ca.* 0.03 Å.[13] Finally different DFT functionals result in lattice constants that differ by a few percent.[29] Our choice of PBEsol is designed to reproduce bond lengths but it still overestimates the bond length in bulk Au by 0.022 Å. This combination of factors can explain the bond length differences seen between DFT and our experimental EXAFS analysis of the Au_{147} particles.

A detailed structural analysis reveals that the fine-structure of the Au–Au bond length distribution depends upon the location of the bonds. From the PDFs, the bond contraction is mainly attributed to the contraction in the surface–core and core–core bonds. The surface–surface bonds in Au_{147}, on the other hand, showed bond elongation. Quantitatively, the average surface–core, core–core, and surface–surface bond lengths are 2.840, 2.850, and 2.904 Å, respectively. Upon the reduction of the coordination number, the bonds in the Au_{147} nanoparticle are not all contracted as predicted by phenomenological models such as the bond-order–length–strength (BOLS) model.[30]

3.5 Vibrational properties

The calculated σ^2 for the Au foil and Au_{147} along with the values obtained by fitting the experimental EXAFS data at multiple temperatures with the Einstein model (eqn (3)) are shown in Fig. 7. There is good agreement between the theoretical and the experimental σ^2 for both the Au foil and Au_{147} DENs. The dynamical part of σ^2 can be well represented by the correlated Einstein model with a fitted Einstein temperature as shown in Fig. 7. Our calculations confirm the experimental trend that the Einstein temperature decreases with the size reduction.

The decrease in the Einstein temperature can be understood from the bond-projected VDOS of Au bulk and Au_{147} as shown in Fig. 8. A notable feature of these data is that the vibrational spectrum of Au_{147} is broader than the Au bulk. Specifically, additional low frequency modes are present in Au_{147} within the acoustic gap of Au bulk and the maximum frequency extends up to above 6 THz in Au_{147} from 4.5 THz of Au bulk. To further resolve the vibrational softening and strengthening, the corresponding VDOS for the three types of bonds are shown in Fig. 8 as well as the characteristic Einstein frequency to characterize the relative strength of the thermal vibrations.[31] It can be seen that the softening comes from the surface–surface bonds where the Einstein frequency drops significantly below the bulk value. On the other hand, bond strengthening is observed in the surface–core and core–core bonds. These behaviors are consistent with the corresponding changes in bond lengths (contraction in the core and elongation at the surface) described in the previous section.

Given that there is both stiffening and softening of the vibrational modes in the nanoparticle compared to the bulk, we may not be able to generally say that the Einstein temperature of the nanoparticles will be lower than the bulk. It is reasonable, however, that when nanoparticles become as small as 147 atoms and there are more surface atoms than in the core, that the softening of modes on the surface will dominate over stiffening in the core.

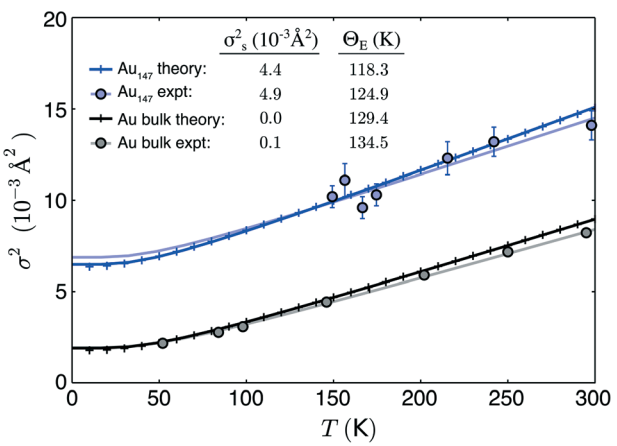

Fig. 7 Debye–Waller factor (σ^2) of Au foil and Au_{147} as a function of temperature. The plus symbols are calculated values from eqn (1) and (2); the circles are obtained through fits to the experimental EXAFS data, both independent of the Einstein model. The solid lines are fits based upon the Einstein model to the calculated (dark lines) and experimental data (light lines).

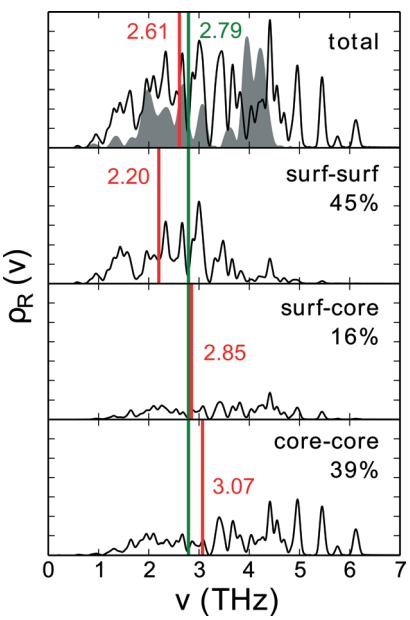

Fig. 8 Bond-projected VDOS. The estimated Einstein frequency is the average of $(\mu_{-1})^{-1}$ and $(\mu_{-2})^{-2}$, where μ_P is the power moment of the normalized vibrational DOS. The red and green vertical lines indicate the Einstein frequencies for Au_{147} and Au bulk, respectively. The shaded VDOS is for Au bulk.

4 Conclusions

In this study, the structural and vibrational properties of Au_{147} DENs are studied by using a combination of EXAFS and the DFT calculations. The structure of Au_{147} DENs is determined to be icosahedral by comparing the simulated and the experimental EXAFS spectrum. Based on the determined structure, the structural and vibrational properties of Au_{147} are analyzed. The Au–Au bond length of icosahedral Au_{147} shows overall contraction compared to the Au bulk. Detailed analysis shows that Au–Au bonds at different locations on the nanoparticle have different relaxation behaviors. The surface–surface bonds exhibit bond expansion, while the surface–core and core–core bonds are contracted. The reduction of the Einstein temperature in Au_{147} is attributed to the softening of vibrational modes for the surface–surface bonds.

Acknowledgements

This work was supported by the National Science Foundation under the DMREF program Grant 1534177 (RMC and GH) and 1534184 (AIF). RMC and GH thank the Robert A. Welch Foundation (Grants F-0032 and F-1841) for support. The authors acknowledge the facilities support provided at the Synchrotron Catalysis Consortium (U.S. DOE Grant No. DE-SC0012335). The atomic structures were rendered using Speck (http://wwwtyro.github.io/speck/), a program authored by Rye Terrell. The computational work was done at the National Energy Research Scientific Computing Center and the Texas Advanced Computing Center.

References

1 A. S. K. Hashmi and G. J. Hutchings, *Angew. Chem., Int. Ed.*, 2006, **45**, 7896–7936.
2 G. C. Bond and D. T. Thompson, *Catal. Rev.: Sci. Eng.*, 1999, **41**, 319–388.
3 B. Hvolbœk, T. V. Janssens, B. S. Clausen, H. Falsig, C. H. Christensen and J. K. Nørskov, *Nano Today*, 2007, **2**, 14–18.
4 N. Lopez, T. Janssens, B. Clausen, Y. Xu, M. Mavrikakis, T. Pedersen and J. Nørskov, *J. Catal.*, 2004, **223**, 232–235.
5 R. B. Getman, Y. Xu and W. F. Schneider, *J. Phys. Chem. C*, 2008, **112**, 9559–9572.
6 F. Behafarid, J. Matos, S. Hong, L. Zhang, T. S. Rahman and B. R. Cuenya, *ACS Nano*, 2014, **8**, 6671–6681.
7 G. Shafai, M. A. Ortigoza and T. S. Rahman, *J. Phys.: Condens. Matter*, 2012, **24**, 104026.
8 T. Castro, R. Reifenberger, E. Choi and R. P. Andres, *Phys. Rev. B: Condens. Matter Mater. Phys.*, 1990, **42**, 8548–8556.
9 P. Buffat and J.-P. Borel, *Phys. Rev. A: At., Mol., Opt. Phys.*, 1976, **13**, 2287–2298.
10 W. Qi and M. Wang, *Mater. Chem. Phys.*, 2004, **88**, 280–284.
11 F. A. Lindemann, *Phys. Z.*, 1910, **11**, 609.
12 A. Yevick and A. I. Frenkel, *Phys. Rev. B: Condens. Matter Mater. Phys.*, 2010, **81**, 115451.
13 S. T. Chill, R. M. Anderson, D. F. Yancey, A. I. Frenkel, R. M. Crooks and G. Henkelman, *ACS Nano*, 2015, **9**, 4036–4042.
14 V. Petkov, N. Bedford, M. R. Knecht, M. G. Weir, R. M. Crooks, W. Tang, G. Henkelman and A. Frenkel, *J. Phys. Chem. C*, 2008, **112**, 8907–8911.
15 R. M. Crooks, M. Zhao, L. Sun, V. Chechik and L. K. Yeung, *Acc. Chem. Res.*, 2001, **34**, 181–190.
16 O. M. Roscioni, N. Zonias, S. W. T. Price, A. E. Russell, T. Comaschi and C.-K. Skylaris, *Phys. Rev. B: Condens. Matter Mater. Phys.*, 2011, **83**, 115409.
17 S. W. T. Price, N. Zonias, C.-K. Skylaris, T. I. Hyde, B. Ravel and A. E. Russell, *Phys. Rev. B: Condens. Matter Mater. Phys.*, 2012, **85**, 075439.
18 D. F. Yancey, S. T. Chill, L. Zhang, A. I. Frenkel, G. Henkelman and R. M. Crooks, *Chem. Sci.*, 2013, **4**, 2912–2921.
19 G. Kresse and J. Furthmüller, *Comput. Mater. Sci.*, 1996, **6**, 15–50.
20 G. Kresse and J. Furthmüller, *Phys. Rev. B: Condens. Matter Mater. Phys.*, 1996, **54**, 11169.
21 P. E. Blöchl, *Phys. Rev. B: Condens. Matter Mater. Phys.*, 1994, **50**, 17953.
22 G. Kresse and D. Joubert, *Phys. Rev. B: Condens. Matter Mater. Phys.*, 1999, **59**, 1758–1775.
23 J. P. Perdew, A. Ruzsinszky, G. I. Csonka, O. A. Vydrov, G. E. Scuseria, L. A. Constantin, X. Zhou and K. Burke, *Phys. Rev. Lett.*, 2008, **100**, 136406.
24 S. I. Zabinsky, J. J. Rehr, A. Ankudinov, R. C. Albers and M. J. Eller, *Phys. Rev. B: Condens. Matter Mater. Phys.*, 1995, **52**, 2995–3009.
25 A. V. Poiarkova and J. J. Rehr, *Phys. Rev. B: Condens. Matter Mater. Phys.*, 1999, **59**, 948–957.
26 F. D. Vila, V. E. Lindahl and J. J. Rehr, *Phys. Rev. B: Condens. Matter Mater. Phys.*, 2012, **85**, 024303.
27 A. I. Frenkel and J. J. Rehr, *Phys. Rev. B: Condens. Matter Mater. Phys.*, 1993, **48**, 585–588.
28 A. I. Frenkel, C. W. Hills and R. G. Nuzzo, *J. Phys. Chem. B*, 2001, **105**, 12689–12703.
29 P. Haas, F. Tran and P. Blaha, *Phys. Rev. B: Condens. Matter Mater. Phys.*, 2009, **79**, 085104.
30 C. Q. Sun, *Prog. Solid State Chem.*, 2007, **35**, 1–159.
31 E. Sevillano, H. Meuth and J. J. Rehr, *Phys. Rev. B: Condens. Matter Mater. Phys.*, 1979, **20**, 4908–4911.